Constructal design applications in buildings: Radiant cooling panels and thermochemical energy storage

Mohamed Mosa, Alexandre Malley-Ernewein

Constructal design applications in buildings: radiant cooling panels and thermochemical energy storage

Mohamed Mosa[a,b], Alexandre Malley-Ernewein[a,*]

[a] *LMDC, Université de Toulouse, UPS, INSA, 135 Avenue de Rangueil, 31077 Toulouse cedex 04 France*
[b] *Department of Mechanical Engineering, Tobruk University, Tobruk, Libya*

Abstract

The present work highlights how the Constructal law is implemented in the search for buildings performance from a thermal lookout. The authors reviewed some of their research efforts through two applications: radiant cooling panels and thermochemical energy storage in buildings. In a deterministic approach, it was demonstrated that the overall performance of such systems could be anticipated. Under the same operating conditions, cooling panel with dendritic flow configurations exhibited better global performance compared to the design with a serpentine flow layout. Two configurations of elemental reactors for thermochemical energy storage were studied: reactive material in beds layers and impregnated within a tube. A theoretical approach allowed to predict the impact of the Bejan number on the sensible heat output for the first configuration, when numerical experiments allowed to determine how to morph the tube shape to increase thermal performances.

Keywords: Constructal law, Radiant cooling panel, Thermochemical energy storage, Efficient design, Buildings, Numerical simulations.

* Corresponding author: malley@insa-toulouse.fr

Nomenclature

Radiant cooling panels

Symbols

A_r	surface ratio
A_θ	surface area at temperature $< \theta$, m^2
c_p	specific heat capacity, J/(kg.K)
D	diameter, m
g	gravitational constant, m^2/s
h	heat transfer coefficient, W/(m^2.K)
I	identity matrix
k	thermal conductivity, W/(m.K)
L	plate length, m
L_c	characteristic length
l	flow path length, m
ṁ	mass flow rate, kg/s
p	pressure, Pa
Q	cooling capacity, W
Ra	Rayleigh number
S	tube spacing, m
Sv	Svelteness number
T	temperature, K
u	velocity vector, m/s
V_{flow}	flow volume, m^3
W	plate width, m
Ẇ	pumping power, W

Greek symbols

Δp	pressure drop, Pa
ε	emissivity
θ	non-dimensional temperature
μ	dynamic viscosity, Pa.s
σ	Stefan–Boltzmann's constant
ρ	density, kg/m^3

Subscripts

a	air
al	aluminum
amb	ambient
in	inlet
p	plate
srp	serpentine

Thermochemical energy storage

Symbols

a	reaction advancement
Be	Bejan number
c	vapor concentration, mol/m^3
c_p	heat capacity, J/(K.kg)
D	channel thickness, m
D	Diffusion coefficient, m²/s
t	time, s
u	velocity vector, m/s
V	volume, m^3
W	module thickness, m

Greek symbols

Δp	pressure difference, Pa

e	impregnated layer thickness, m	μ	dynamic viscosity, Pa.s
H	module height, m	ε	porosity
K	permeability, m^2	ρ	density, kg/m^3
k	thermal conductivity, W/(K.m)		
k_{cin}	reaction kinetic coefficient, s^{-1}	*Subscripts*	
k_{sto}	reaction stoichiometric coefficient	0	initial
L	module length, m	eff	effective
L	Tube length, m	eq	equilibrium
M	Molar mass, kg/mol	f	fluid
$\dot{m}$	mass flow rate, kg/s	i	inner
n	bulk density, mol/m^3	in	inlet
p	Pressure, Pa	max	maximal
R	tube channel radius, m	out	outlet
T	temperature, K	s	salt

1. Introduction

Since it was first introduced two decades ago, the Constructal law has been widely applied in the search for better performance of systems crossed by flows. If the studies began on the street network design[1], the principal field of application became heat and mass transfer[2–7]. Thus some buildings-related thermal applications can be found in the literature[8–13]. In France, space heating represents almost two third of the energy consumption[14] of residential buildings: increasing the systems efficiency can be a suitable way to reduce the energy consumption.

Here, two examples of the authors' current research activities considering the applications of the Constructal law in the context of thermal systems in the buildings sector are reviewed. In light of the Constructal law and Second Law Conference 2019, the topics consider radiant cooling panels and energy storage in buildings.

1.1. Ceiling radiant panels for cooling applications

Because of their low energy demand compared to air conditioning systems, radiant panels systems studies have been increasing with the aim of reducing the buildings footprint on the environment. A ceiling radiant panel is made of a metal plate insulated from the top and sides surfaces while its lower surface exchanges heat with the surroundings, mainly by radiation. To maintain the required indoor thermal comfort, radiant panels are equipped with flow channels, fixed to the upper side of the metal plate, through which water circulates to remove the heat gained by the plate. The serpentine flow layout is generally employed in radiant panels systems.

A great effort has been made in previous published work concerning radiant panel systems to evaluate the performance of radiant ceiling panels in terms of thermal comfort and energy saving potentials compared to air conditioning systems. This was achieved at the room scale. However, the problem is multiscale in nature: room scale & panel scale. Therefore, the focused

in the reported work by Mosa *et al.*[15,16] was on addressing the problem form a fundamental perspective at the scale of the panel. The objective was to investigate the overall performance of single panel unit equipped with different flow architectures. It was demonstrated that morphing both the flow architectures and the panel shape led to better global performance. An almost square panel deign provided higher cooling capacity to pumping power ratio. Taking a nearly square panel shape (aspect ratio of 1.05) as an example, in this work, the authors illustrate how the Construcal design approach was implemented for efficient panels design practice.

1.2. Thermochemical energy storage

Increasing the share of renewable energy in buildings is a European Union objective for the next decades[17,18]. However, an issue related to renewable energy is the mismatch between production and consumption periods. This mismatch calls for thermal energy storage techniques in order to satisfy the consumer needs. The gap between production and consumption led to research in energy storage methods of several kinds[19]: sensible, latent or thermochemical.

The latter reaction involves a salt and its hydrate, and the energy released comes from the latent enthalpy and the bonds dissociation enthalpy during the hydration and dehydration processes.

Nevertheless, before being applied in buildings, thermochemical energy storage system needs to be more efficient.

Thus designs of thermochemical energy reactors were studied under the Constructal law scope in 2 different configurations[20,21]: at the module scale[20], in a configuration with the reactive material is divide in beds in the volume, at an elemental component scale[21], in a configuration with the reactive material impregnated into a tube. The objectives of these previous works were to determine design trends, leading to efficient systems, through a theoretical approach and to confirm them using numerical experiments.

2. Methodology

2.1. Ceiling radiant panels

2.1.1 Panel unit configurations

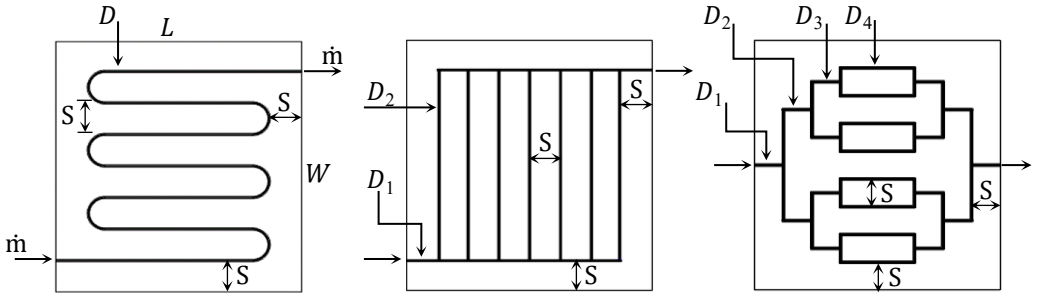

Figure 1 Flow architectures: (a) serpentine, (b) canopy-to-canopy and (c) tree-shaped - Figure adapted from previous work[16].

The serpentine design portrayed in Fig. 1 (a) is made of a single tube of a diameter D and a flow path length l. As opposed to the serpentine design, by applying a Constructal approach, two tube diameters were employed in a canopy-to canopy configuration, Fig.1 (b), which is a special case of the tree-shaped design. The degree of freedom was further increased with multiple-channel size for the tree-shaped structure depicted in Fig.1 (c).

The Constructal design approach establishes that for flow systems with large svelteness, Sv, ($>$ 10) the local pressure losses can be neglected[22,23]. As described in Ref.[15,16], for the current panels with branching flow structures, as given by Eq. (11), Sv $=$ 26.

$$\mathrm{Sv} = \frac{l}{V_{\mathrm{flow}}^{1/3}}\, W/L \tag{1}$$

For laminar flow in circular ducts, the ratio $\dot{\mathrm{W}}/\dot{\mathrm{m}}^2$ is proportional to $1/D^4$. For a fixed V_{flow}, the optimum ducts diameters for minimum $\dot{\mathrm{W}}$ can be obtained by invoking the Lagrange multipliers method to find the extremum of the aggregate function

$$\varphi = \frac{\dot{\mathrm{W}}}{\dot{\mathrm{m}}^2} + \lambda(V_{\mathrm{flow}}) \tag{2}$$

where λ is the Lagrange multiplier[12].

For the canopy-to-canopy configuration, Fig.1 (b), the main flow rate, $\dot{\mathrm{m}}$, feeds seven evenly spaced parallel segments. Here $\dot{\mathrm{W}}/\dot{\mathrm{m}}^2$ can be expressed as follows

$$\frac{\dot{\mathrm{W}}}{\dot{\mathrm{m}}^2} = \left[\frac{\left(2 + \sum_{i=1}^{6} i/7\right)\mathrm{S}}{{D_1}^4} + \frac{(W - 2\,\mathrm{S})}{7\,{D_2}^4}\right] \tag{3}$$

For this design, V_{flow} can be expressed as

$$V_{\mathrm{flow}} \sim 2\,(L - \mathrm{S})\,{D_1}^2 + 7\,(W - 2\,\mathrm{S})\,{D_2}^2 \tag{4}$$

The diameter ratio, D_{r}, for the least pumping power penalty corresponds to

$$D_{\mathrm{r}} = \frac{D_1}{D_2} = \left[\frac{245\,\mathrm{S}}{2\,(L - \mathrm{S})}\right]^{1/6} \tag{5}$$

In similar fashion, for the tree-shaped structure displayed in Fig.1 (c), Bejan and Lorente[23] showed that that D_{r} is 1.26. This ratio applies to the diameters before and after any bifurcation level.

2.1.2 Model

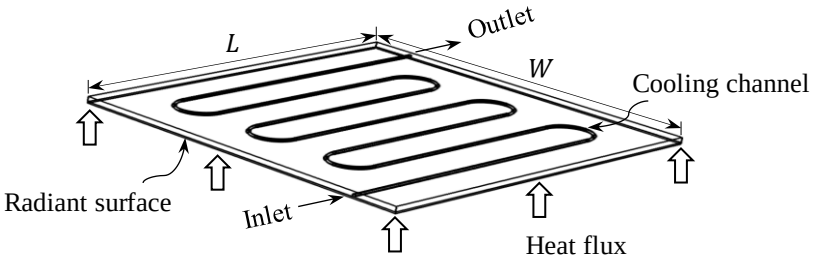

Figure 2 Cooling panel - Adapted from previous work[15].

As presented in Fig. 2, water at fixed flow rate, $\dot{m}$, and temperature, $T_{\mathrm{w,in}}$, enters the panel to extract the heat absorbed by the lower side of the plate. The panel is presumed to cool an ambient at a controlled temperature, T_{amb}. The total sensible heat flux to the panel depends on the energy balance between the conditioned zone and the panel. It was estimated as the average of the local radiation and convection fluxes.

$$\boldsymbol{\nabla}\mathbf{u} = 0 \tag{6}$$

$$\rho_{\mathrm{w}}\,(\mathbf{u}\boldsymbol{\nabla})\mathbf{u} = \boldsymbol{\nabla}[-p\mathbf{I} + \mu_{\mathrm{w}}(\boldsymbol{\nabla}\mathbf{u})] \tag{7}$$

$$\rho_{\mathrm{w}}\,c_{p,\mathrm{w}}\,\mathbf{u}\,\boldsymbol{\nabla}T + \boldsymbol{\nabla}(-k_{\mathrm{w}}\boldsymbol{\nabla}T) = 0 \tag{8}$$

$$\boldsymbol{\nabla}(-k_{\mathrm{al}}\boldsymbol{\nabla}T) = 0 \tag{9}$$

where $\mathbf{u}$ is the fluid velocity field, p is the pressure, $\mathbf{I}$ is the identity matrix, and T is the temperature. ρ_{w}, μ_{w}, $c_{p,\mathrm{w}}$, and k_{w} are the density, dynamic viscosity, specific heat, and thermal conductivity of the water, respectively. k_{al} is the thermal conductivity of the aluminum plate.

For laminar water flow, the continuity equation, Eq. (6), the Naiver-stokes, Eq. (7), and the energy equation, Eq. (8), were solved alongside the energy equation for the aluminum plate domain, Eq. (9).

Table 1 Details of the panel and operating conditions (reference[15])

Details of the panel				Operating conditions		
W/L (-)	$W \times L$ (m^2)	ε_p (-)	V_{flow} (m^3)	$\dot{m}$ (kg/s)	$T_{w,in}$ (°C)	T_{amb} (°C)
1.05	1.35	0.9	5.64×10^{-4}	0.004	15	24

where W/L is the aspect ratio, $W \times L$ is the plate area, ε_p is the emissivity of the lower side of the plate, and V_{flow} is the volume allocated to the flow.

The cooling performance of a panel furnished with serpentine, canopy-to-canopy and tree-shaped flow architectures was numerically explored. As presented in Table 1, the same operating conditions was applied to all the configurations. The top and side surfaces of the panel are assumed adiabatic. The cooling capacity represents the total sensible heat absorbed by the lower side of the plate (due to radiation and convection heat exchanges with the surrounding), which can be estimated as

$$Q = \left[\varepsilon_p \, \sigma \left(T_{amb}^4 - T_p^4\right) + h \left(T_{amb} - T_p\right)\right](W \times L) \qquad (10)$$

with h, the heat transfer coefficient for natural convection air flow, estimated as[24]

$$h = \frac{k_a}{L_c} 0.15 \, \mathrm{Ra}_{L_c}^{1/3} \qquad (11)$$

where k_{a} is the thermal conductivity of the air, L_c is the characteristic length scale of the plate, and Ra_{L_c} represents the Rayleigh number.

The most efficient panel design was identified in terms of cooling capacity, Q, pumping power demand, $\dot{\mathrm{W}}$, and surface temperature distribution, $A_r(\theta)$ as discussed below. The pumping power demand to drive the water across the panel is defined as

$$\dot{\mathrm{W}} = \frac{\Delta p\ \dot{\mathrm{m}}}{\rho_{\mathrm{w}}} \tag{12}$$

where Δp is the pressure drop from inlet to outlet of the flow architecture.

Considering the panel with the serpentine flow arrangement as a reference, an overall performance indicator, η, was introduced. As defined in Eq. (8), η represents the ratio of cooling performance to the pumping power demand compared to the reference case.

$$\eta = \frac{Q - Q_{\mathrm{srp}}}{\dot{\mathrm{W}} - \dot{\mathrm{W}}_{\mathrm{srp}}} \tag{13}$$

where Q_{srp} and $\dot{\mathrm{W}}_{\mathrm{srp}}$ designates in turn the cooling capacity and the pumping power for panel equipped with the serpentine flow layout.

Finally, the temperature distribution on the surface of the plate was evaluated as $A_r(\theta)$, with θ and A_r defined as follows

$$\theta = \frac{T_{\mathrm{p}} - T_{\mathrm{w,in}}}{T_{\mathrm{amb}} - T_{\mathrm{w,in}}} \tag{14}$$

$$A_r = \frac{A_\theta}{W \times L} \tag{15}$$

where A_θ represents the surface area where the temperature is $\leq \theta$.

A 3D steady state numerical solution was obtained with a finite element method (FEM) software package[25] running on a CPU using Intel(R) Xeon(R) (2 processors at 2.30 GHz) with 64 GB of RAM.

A mesh independency study was performed to ensure that the numerical solution is not mesh dependent following the procedure described in the previous work[15,16]. For the geometry depicted in Fig. 1 (a), the panel with the serpentine flow design, the computational domain consists of 3.59×10^4 prism meshing elements. For the canopy-to-canopy configuration portrayed in Fig. 1 (b), the domain contains 8.08×10^4 meshing elements (3.66×10^4 tetrahedral and 4.42×10^4 prism). As the tree-shaped panel design, Fig. 1 (c) possess a symmetry, half of the geometry was simulated. The considered model is made up of 7.46×10^4 meshing elements (4.67×10^4 tetrahedral and 2.79×10^4 prism).

To ensure that the numerical solution is stabilized and computationally cost-effective, consistent stabilization methods are used. In this way, artificial diffusions are added only where desired (in the regions where the mesh is not fine enough) to guarantee that the element Péclet number is < 1. The simulations were conducted with relative tolerance of 10^{-3}.

Using second-order (quadratic) discretization element for the velocity found not to influence the numerical results (pressure drop and temperature) for all the panel configurations. However, a significant jump in the number of degrees of freedom (DOF) was observed, and hence, calculation time and computational resources increased. For example, for the tree-shaped design shown in Fig. 1 (c), the number of DOF was 1.22×10^5 with the linear element and increased to 5.35×10^5 with the quadratic element. As a result, the physical memory requirement increased from 2.03 to 7.12 GB and the calculation time jumped from 127 to 884 s with the quadratic element. More details on the numerical techniques are given in the reference[26].

2.2. Thermochemical energy storage

2.2.1 Storage unit configurations

In the work previously done[20], two configurations of thermochemical energy storage unit were studied in an open process; the heat transfer fluid is humid air and the reactants are water vapor (carried by air) and strontium bromide.

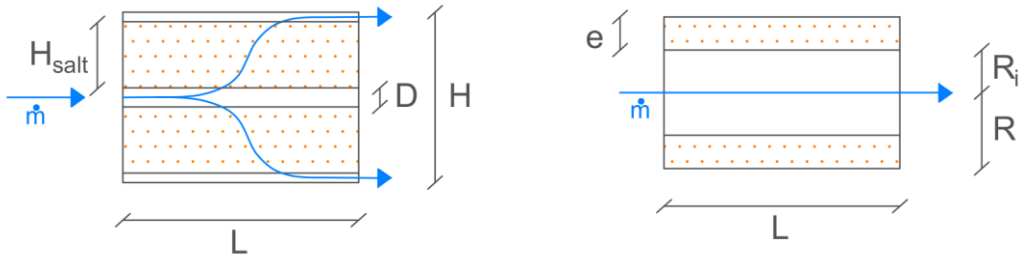

Figure 3 Cross-sectional view of the two studied configurations, the 1st with air flow perpendicular to the salt (left), and the 2nd with air flow parallel to the salt (right), studied in previous work[20].

The first configuration explored[20] is an elemental module with the reactive material divided into two beds. The total and salt volumes are fixed as $V = WLH$ and $V_s = H_sWL$, where H_s is one salt layer height. Fluid channels of thickness D are inserted between the salt beds, and the channels at the two ends of the volume have a thickness $D/2$. In this configuration, the fluid flow enters from the left (see Fig. 3) and follows the channel which end is obstructed, forcing the fluid to pass through the adjacent salt beds. At the exit of the salt bed, the fluid is again channeled and exits on the other side of the module. The mass flow rate $\dot{m}$ is fixed.

The second configuration studied is a cylinder of length L and radius R. Along the inner wall of the cylinder, a fixed salt volume is uniformly impregnated at a thickness e. The followings assumptions are made: the deposited layer is done at the grain scale and the water vapor only

diffuses through it. Thus the air flow is blown inside a channel of radius R_i formed by the salt layer, sweeps it and water vapor diffuses within, allowing the hydration or dehydration reaction to occur. The volumes can be expressed as $V = \pi R^2 L$ and $V_s = \pi(R^2 - R_i^2)L$. The two configurations are presented in Fig. 3.

The concepts are investigated under the scope of the Constructal law. Theoretical approach with analysis of the physical phenomena is coupled with numerical experiments.

2.2.2 Model

In order to study the concept of the two thermochemical open reactors, a set of equations was developed to describe the heat and mass transfers. This model is nearly the same for the two configurations. The difference is in the water vapor transport mode in the salt layer: by convection through the salt bed for the first configuration and pure diffusion through the salt grains in the second.

In the channels, the mass conservation for humid air (Eq. (16)) and for the water vapor (Eq. (17)) were solved. The air flow in the channels is laminar (Eq. (18)). To complete the set of equations common to both configurations, the energy conservation is written (Eq. (19)).

$$\frac{D\rho}{Dt} = 0 \tag{16}$$

where ρ is the humid air density.

$$\frac{Dc}{Dt} + \boldsymbol{\nabla}(-D_v \boldsymbol{\nabla} c) = 0 \tag{17}$$

where c is the water vapor concentration, and D_v is the vapor diffusion coefficient.

$$\rho \frac{D\boldsymbol{u}}{Dt} = -\boldsymbol{\nabla} p + \mu \boldsymbol{\nabla}^2 \boldsymbol{u} \tag{18}$$

where $\boldsymbol{u}$ is the velocity vector and p the pressure.

$$\rho c_p \frac{DT}{Dt} + \boldsymbol{\nabla} \cdot (k \boldsymbol{\nabla} T) = 0 \quad (19)$$

Mass conservation for humid air in the salt is solved only in the first configuration (Eq. (20)). To couple with the Navier-Stokes equation used in the channels, the Brinkman equation (Eq. (21)) is used, describing the momentum conservation. The water vapor conversation in the salt is solved in both cases (Eq. (22)) with only diffusion in the second case. Thus $\boldsymbol{u} = 0$ and there is no porosity in the reactive material, the intra diffusion coefficient is taken to 1.2×10^{-13} m²/s [27]. The source/sink due to the salt dehydration/hydration is modelized by the term in the right hand side of Eqs. (20) and (22). The energy conservation is written with a heat source/sink due to the chemical reaction in the salt (Eq. (23a)) and modified for the second configuration (Eq.(24b)).

$$\varepsilon \frac{\partial \rho}{\partial t} + \boldsymbol{\nabla}(\rho \boldsymbol{u}) = -k_{sto}\, n_s \frac{da}{dt} M_v \quad (20)$$

$$\rho \frac{D\boldsymbol{u}}{Dt} = \varepsilon \left[-\boldsymbol{\nabla} p + \mu \boldsymbol{\nabla}^2 \boldsymbol{u} + \frac{\mu}{K} \boldsymbol{u} \right] \quad (21)$$

$$\varepsilon \frac{\partial c}{\partial t} + \boldsymbol{\nabla}\left(-D_{v,eff} \boldsymbol{\nabla} c\right) + \boldsymbol{u}\, \boldsymbol{\nabla} c = -k_{sto}\, n_s \frac{da}{dt} \quad (22)$$

where $D_{v,eff}$ is the effective diffusion coefficient of the water vapor in the air inside the porous medium, and M_v is the molar mass of vapor.

$$\left(\rho c_p\right)_{eff} \frac{\partial T}{\partial t} + \rho c_p \boldsymbol{u} \cdot \boldsymbol{\nabla} T + \boldsymbol{\nabla} \cdot \left(k_{eff} \boldsymbol{\nabla} T\right) = n_s \frac{da}{dt} \Delta h \quad (23a)$$

$$c_{p_s} \frac{\partial T}{\partial t} + \boldsymbol{\nabla} \cdot (k_s \boldsymbol{\nabla} T) = n_s \frac{da}{dt} \Delta h \quad (24b)$$

where $\left(\rho c_p\right)_{eff}$ and k_{eff} are the effective characteristics of the porous medium[28]. Δh is the reaction enthalpy. The reaction advancement rate da/dt is given by:

$$\frac{da}{dt} = k_{cin}\left(1 - \frac{p_{eq}}{p_v}\right)(1 - a) \quad (25)$$

The boundary conditions are: fixed water vapor concentration c_{in}, fixed temperature T_{in} at the channels entrance. At the channel outlet, an outflow condition is applied as a boundary condition for the heat transfer and the vapor transport, and atmospheric pressure is applied for the fluid. For all the external boundaries the conditions used are: thermal insulation, no-slip velocity, and zero vapor flux.

At $t = 0$, the temperature of the entire system is equal to T_0, the fluid is at rest and at atmospheric pressure, c_0 is the vapor concentration corresponding to the equilibrium vapor pressure at the initial temperature.

The equations system is solved thanks to a finite element software[25] and the energy and mass conversation were used as verification criteria for the model meshing.

Unsteady solutions were obtained with a finite element method (FEM) software package[25] running on a CPU using Intel(R) Xeon(R) with 2 processors at 3.00 GHz and 128 GB of RAM.

Due to the system geometry, only one bed behavior was modelized at the module scale, in 2D. Depending the geometry of the system, the mesh was composed between 1.3×10^4 and 4.6×10^4 triangular elements. At the elemental component scale, the mesh was composed by triangular elements, between 8.0×10^4 and 1.2×10^5 with a 2D axial symmetry to reconstruct the tube solutions. To ensure that the numerical solution is not mesh dependent a mesh independency study was performed by the authors. First order discretization was used to solve velocity and pressure calculation in fluid domains for both configurations, when second order discretization was used to solve velocity in porous domain in the first configuration.

Models were launched for 300 simulated hours in the 1st configurations and 1 000 simulated hours for the 2nd configuration. The calculation time steps depended to the solutions convergence, with a maximal of 1h. Storage time steps were 1h in both cases.

3 Results and discussion

3.1. Ceiling radiant panels

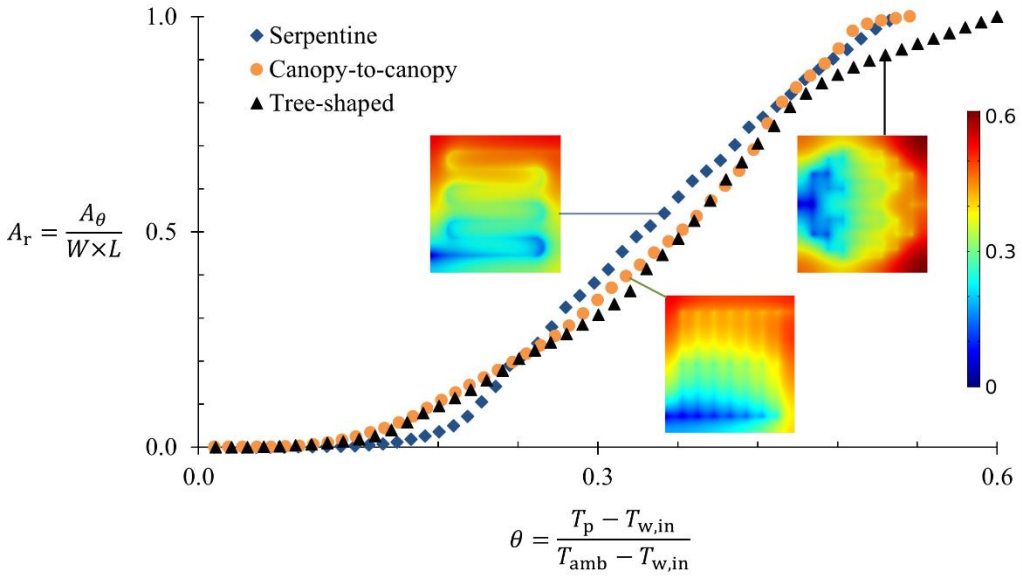

Figure 4 Temperature distribution on the radiant surface of the panel - Adapted from previous work[15,16].

The temperature distribution on the surface of the plate is plotted in Fig. 4. Water gains heat as it crosses the panel and the temperature of the plate surface rises therefore along the flow path. A concentration of cold spot (near the inlet) and hot spot (near the outlet) is noticeable. The

temperature spread was slightly wider with the tree-shaped design. For all the flow architectures, the average temperature of the plate surface, θ_{pm}, was in similar magnitude.

The panels provided similar cooling capacities, Q. Radiation accounted for about 60% of the heat flux received by the plate. The Constructal designs shortened the flow path, $\tilde{l}$, by 0.69 compared to the serpentine layout. For the same flow rate, this ensured more than 90% saving in the pumping power, $\dot{\mathrm{W}}$, required to drive the water across the flow network. Compared to the design with the serpentine flow arrangement, the advantage in the cooling performance over the pumping power requirement, η, with tree-shaped configurations were significant. The dendritic flow patterns shown in Fig. 1 (c) was the most performing design. This a result of allowing the flow structure to change in time by adding more degree of freedom; here it means adding diameters. Table 2 below summarizes the overall results.

Table 2 Summary of results

Flow configuration	D_{r} (-)	$\tilde{l}$ (-)	θ_{pm} (-)	Q (W)	$\dot{\mathrm{W}} \times 10^4$ (W)	η (-)
Serpentine	-	1	0.35	67.58	5.98	-
Canopy-to-canopy	1.61	0.31	0.35	67.09	0.54	901
Tree-shaped	1.26	0.31	0.36	65.66	0.50	3504
where $\tilde{l} = \dfrac{l}{l_{\mathrm{srp}}}$						

As demonstrated here, applying a Constructal approach showed that the design of radiant panels can be improved. For the same cooling performance, compared to the serpentine flow layout, the dendritic flow patterns exhibited noteworthy saving advantages in the pumping power

requirements. Consequently, the cooling capacity to pumping power ratio (thermal over hydraulic performance) can be enhanced.

In current design practice, radiant panels generally cover large surface area (if not the entire available ceiling area). A radiant panel is typically equipped with a serpentine flow channel. This flow arrangement is associated with high-pressure drop across the water network, and therefore, high pumping power demand is expected. The distribution and number of cooling panels in a conditioned space could be considered for further work to assess the merits of the dendritic flow configurations at the scale of the room.

3.2. Thermochemical energy storage

3.2.1 First configuration: theoretical approach

To work on this configuration, the chemical reaction process happening in the salt layer was explored. The heat source due to this reaction can be expressed as the heat transfer rate through a salt slab of thickness H_s, $\dot{q} = \frac{\dot{m}}{2} c_p (T_{out} - T_{in})$. At the slab entrance and exit the fluid temperature is considered equal to the salt bed inlet and outlet temperature, T_{in}, and T_{out} respectively. The reacting bed is assumed as a porous medium, thus the mean velocity is following the Darcy equation, $V = \frac{K}{\mu} \frac{\Delta p}{H_s}$, where Δp is the pressure difference through the salt and K is the salt permeability. Finally, the total heat transfer rate can be expressed as:

$$\dot{q} = k_{eff}\, Be \frac{WL}{H_s} (T_{out} - T_{in}) \qquad (26)$$

where $Be = K\Delta p / \alpha\mu$ is the Be number for porous media[29], α is the thermal diffusivity and k_{eff} is the porous material thermal conductivity[28]. Combining with $\dot{q} = \frac{dc}{dt} \Delta h\, WLH_s$, we obtained:

$$T_{out} - T_{in} = \frac{n_s \, \Delta h \, H_s^2}{k_{eff} Be} k_{cin} \left(1 - \frac{p_{eq}}{p_v}\right)(1 - a) \qquad (27)$$

Or, in a non-dimensional form

$$\frac{\tilde{T}_{out}}{\tilde{T}_{out,max}} = \frac{1}{Be}\left(1 - \frac{p_{eq}}{p_v}\right)(1 - a) \qquad (28)$$

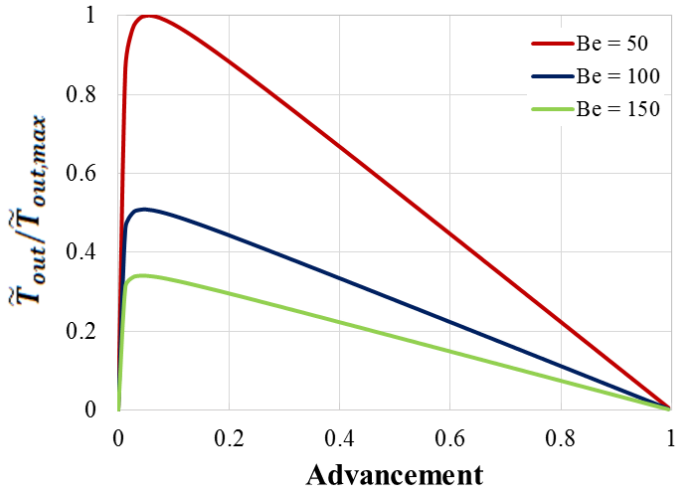

Figure 5 Non-dimensional sensible heat at the exit of a salt bed for various values of the Be number - Adapted from previous work[20].

The evolution of the non-dimensional sensible heat as a function of the reaction advancement for several *Be* number is presented in Fig. 5.

The impact of the Bejan number on the salt bed outlet sensible heat, during the whole reactive material hydration process from a = 0 to a = 1, is highlighted in Fig. 5. Therefore to obtain a higher sensible heat transfer at the exit of the salt layer, consequently at the module exit, the *Be* number has to be decreased.

3.2.2 Second configuration: numerical experiments

To study numerically the second configuration, the tube shape was allowed to morph while fixing the salt volume together with the fluid volume. As the volumes are prescribed, the channel length and tube radius are linked by $V_s = \pi(R_i + e)^2 L - V_f$.

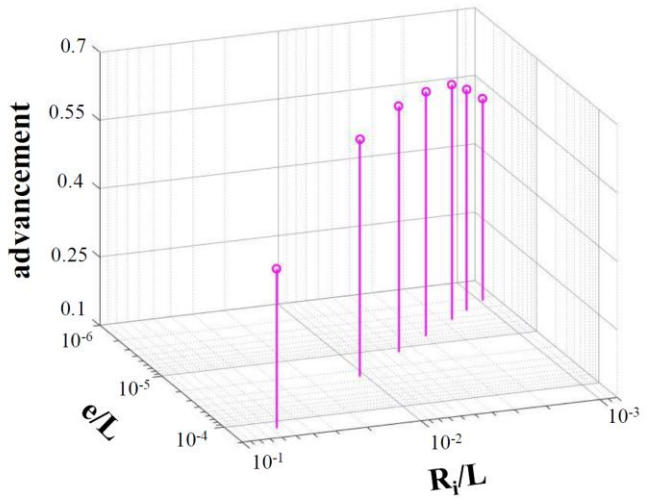

Figure 6 The reaction advancement as a function of the shape ratios e/L and Ri/L with fixed salt and fluid volumes at t/t(a=1) = 0.141 - Adapted from previous work[21].

In Fig. 6, the evolution of advancement for various ratios R_i/L and e/L for a d-less time is presented. For other values of time the trends are identical: the time ($t / t_{(a=1)}$= 0.141) was chosen for illustration reasons.

The impact of the tube geometry on the advancement, hence the system performance, is shown in this Figure. When the salt and fluid volumes are maintained constant, is it possible to define

the geometric ratio in order to design the tubes and to obtain the desired performance. Here the tube with fastest reaction kinetic has shape ratios $Ri/L \sim 3\times10^{-3}$ and $e/L \sim 7\times10^{-6}$.

As demonstrated here and in the previous work[20,21], the Constructal approach coupled to numerical experiments leads to determine more efficient designs for thermochemical energy reactors, at a module scale and at an elemental component scale.

The theoretical approach highlights the Bejan number on the outlet temperature in the first configuration, when the numerical approach leads to determine geometric ratio to obtain a faster reaction in the second configuration. To be useful, thermochemical energy reactors must respond to needs, in term of output heat power and output temperature. Thus, knowing the impact of the system parameters on the outputs is essential to produce adapted reactor.

Assembly of elemental tubes could be considered for further work: to compare impregnated and beds configurations at the scale of the module.

4. Conclusion

The objective of this review was to highlight some of the authors' work on the Constructal law applied toward more efficient energy usage in the building field. The presented results from two different design concepts: cooling panel and thermochemical energy storage. The reviewed work demonstrated that applying a Constructal approach to predict the overall performances of thermal systems is a way to facilitate the design.

The overall performance of a cooling panel equipped with serpentine and dendritic flow designs was evaluated under identical operating conditions and geometrical constraints. The Constructal

flow structures clearly led to dramatically better combined performance relative to the serpentine flow layout. This was attributed to the substantial reduction in the pumping power demand.

The Constructal approach to a thermochemical energy storage module where the reactive material is divided in beds, highlighted the impact of the Bejan number on the reactor output sensible heat. For a reactor configuration with pure diffusion for vapor transport in the reactive material, when the fluid volume is fixed together with the salt volume, it was shown thanks to numerical experiments how the tube shape should be morphed to increase the thermal performances.

Acknowledgements

- Mohamed Mosa was sponsored by the Libyan scholarship program.
- Alexandre Malley-Ernewein's research was funded by the French National Research Agency (ANR – Agence National de la Recherche) DECARTH, ANR-16-CE22-0006-03.

References

1. Bejan, A. Street network theory of organization in nature. *J. Adv. Transp.* **30**, 85–107 (1996).
2. Bejan, A. Constructal-theory network of conducting paths for cooling a heat generating volume. *Int. J. Heat Mass Transf.* **40**, 799–816 (1997).
3. Ledezma, G. A., Bejan, A. & Errera, M. R. Constructal tree networks for heat transfer. *J. Appl. Phys.* **82**, 89–100 (1997).

4. Bejan, A. Constructal tree network for fluid flow between a finite-size volume and one source or sink. *Rev. Générale Therm.* **36**, 592–604 (1997).
5. Lorente, S., Wechsatol, W. & Bejan, A. Fundamentals of tree-shaped networks of insulated pipes for hot water and exergy. *Exergy Int. J.* **2**, 227–236 (2002).
6. Rocha, L. A. O., Lorente, S. & Bejan, A. Constructal design for cooling a disc-shaped area by conduction. *Int. J. Heat Mass Transf.* **45**, 1643–1652 (2002).
7. Wechsatol, W., Lorente, S. & Bejan, A. Tree-shaped insulated designs for the uniform distribution of hot water over an area. *Int. J. Heat Mass Transf.* **44**, 3111–3123 (2001).
8. Trancossi, M., Stewart, J., Dumas, A., Madonia, M. & Marques, J. P. Constructal Design of an Entropic Wall With Circulating Water Inside. *J. Heat Transf.* **138**, (2016).
9. Lui, C. H., Fong, N. K., Lorente, S., Bejan, A. & Chow, W. K. Constructal design of evacuation from a three-dimensional living space. *Phys. Stat. Mech. Its Appl.* **422**, 47–57 (2015).
10. Miguel, A. F. Constructal design of solar energy-based systems for buildings. *Energy Build.* **40**, 1020–1030 (2008).
11. Biserni, C. & Garai, M. First and second law analysis applied to building envelope: A theoretical approach on the potentiality of Bejan's theory. *Energy Rep.* **1**, 181–183 (2015).
12. Biserni, C. & Garai, M. Energy balance and second law analysis applied to buildings: an opportunity for Bejan's theory. *Int. J. Heat Technol.* **34**, S185–S187 (2016).
13. Mutani, G., Todeschi, V., Grisolia, G. & Lucia, U. Introduction to Constructal Law Analysis for a Simplified Hourly Energy Balance Model of Residential Buildings at District Scale. *Tec. Ital.-Ital. J. Eng. Sci.* **63**, 13–20 (2019).
14. ADEME. Qui consomme le plus d'énergie en France ? *ADEME* https://www.ademe.fr/en/particuliers-eco-citoyens/dossiers-comprendre/dossier/lenergie-france/consomme-plus-denergie-france (2018).

15. Mosa, M., Labat, M. & Lorente, S. Role of flow architectures on the design of radiant cooling panels, a constructal approach. *Appl. Therm. Eng.* **150**, 1345–1352 (2019).
16. Mosa, M., Labat, M. & Lorente, S. Constructal design of flow channels for radiant cooling panels. *Int. J. Therm. Sci.* **145**, 106052 (2019).
17. European Union. DECISION No 406/2009/EC OF THE EUROPEAN PARLIAMENT AND OF THE COUNCIL of 23 April 2009 on the effort of Member States to reduce their greenhouse gas emissions to meet the Community's greenhouse gas emission reduction commitments up to 2020. *Official Journal of the European Union* (2009).
18. European Union. European Council (23 and 24 October 2014) – Conclusions. *European Council conclusions* (2014).
19. Solé, A., Martorell, I. & Cabeza, L. F. State of the art on gas–solid thermochemical energy storage systems and reactors for building applications. *Renew. Sustain. Energy Rev.* **47**, 386–398 (2015).
20. Malley-Ernewein, A. & Lorente, S. Constructal design of thermochemical energy storage. *Int. J. Heat Mass Transf.* **130**, 1299–1306 (2019).
21. Malley-Ernewein, A. & Lorente, S. Analysis of thermochemical energy storage in an elemental configuration. *Sci. Rep.* **9**, 1–9 (2019).
22. Lorente, S. & Bejan, A. Svelteness, freedom to morph, and constructal multi-scale flow structures. *Int. J. Therm. Sci.* **44**, 1123–1130 (2005).
23. Bejan, A. & Lorente, S. *Design with Contructal Theory*. (John Wiley & Sons, 2008).
24. Bejan, A. *Convection heat transfer*. vol. 1 (John Wiley & Sons, Iinc., 1995).
25. *COMSOL Multiphysics*.
26. COMSOL, Inc. COMSOL Multiphysics Reference Manual, version 5.3.
27. Esaki, T. & Kobayashi, N. Reaction Rate Characteristics of SrBr2 Hydration System for Chemical Heat Pump Cooling Mode. *J. Mater. Sci. Chem. Eng.* **04**, 106 (2016).

28. Michel, B., Neveu, P. & Mazet, N. Comparison of closed and open thermochemical processes, for long-term thermal energy storage applications. *Energy* **72**, 702–716 (2014).
29. Nield, D. A. & Bejan, A. *Convection in Porous Media*. vol. 1 (Springer, 1998).